FISEVIER

Contents lists available at ScienceDirect

## Deep-Sea Research Part I

journal homepage: www.elsevier.com/locate/dsri



# Productivity and sediment focusing in the Eastern Equatorial Pacific during the last 30,000 years



Nivedita Thiagarajan a,\*, Jerry F. McManus b

- <sup>a</sup> California Institute of Technology, 1200 E California Blvd, Pasadena, CA 91125, United States
- <sup>b</sup> Lamont-Doherty Earth Observatory, Columbia University, Palisades, NY, USA

#### ABSTRACT

The Eastern Equatorial Pacific (EEP) affects the ocean-atmosphere exchange of CQon seasonal and interannual time scales through a balance of upwelling of CQ rich waters and the drawdown of CO2 by biological productivity in the surface waters. The EEP accounts for almost 3/4ths of the global oceanic outgassing of CO2 to the atmosphere, and it is known that the size of this EEP source of CO<sub>2</sub> varies significantly during El Niño events (Feely et al., 1999). There has been much effort to determine the El Niño Southern Oscillation (ENSO) state of the Equatorial Pacific during the past, particularly at the Last Glacial Maximum (LGM) when the global atmospheric [CO2] was low, yet the glacial ENSO state remains a source of considerable controversy (Ford et al., 2015; Herguera, 2000; Koutavas et al., 2002; Loubere et al., 2004; Lyle, 1988; Paytan et al., 1996; Pedersen, 1983; Sarnthein et al., 1988). Reconstructing past changes in equatorial productivity could help establish the prevailing ENSO state of the Pacific during the LGM, as the El Niño-related deepening of the thermocline in the East Pacific reduces productivity in the EEP and increases it in the Western Equatorial Pacific. Here we investigate changes in productivity in four cores from the equatorial Pacific, modern equatorial cold tongue. We determine changes in productivity using measurements of <sup>231</sup>Pa, <sup>230</sup>Th, <sup>232</sup>Th, and <sup>238</sup>U along with sedimentary fluxes. We also compare our findings to other sediment cores in the Pacific. We find elevated ( <sup>231</sup>Pal<sup>230</sup>Th)<sub>xs</sub> values (higher than production values) in general across the cores, indicating a net sink for oceanic <sup>231</sup>Pa in the EEP. We also find evidence for low levels of lateral sediment focusing, as well as lower productivity during the glacial in reduced <sup>230</sup>Th-normalized opal fluxes and decreased (<sup>231</sup>Pa/<sup>230</sup>Th)<sub>xs</sub> at multiple sites. Examination of authigenic uranium at our sites in conjunction with previous work (Jacobel et al., 2017) shows that between 2 and 3.5 km depth in the Equatorial Pacific, there was a floating pool of respired carbon associated with the southward return flow of North Pacific Deep Water, sequestering CO<sub>2</sub> from the atmosphere during the LGM. We also compile Pacific basin wide records of productivity and Pa/Th during the Holocene (0-11kya) and LGM (18-22kya) and find evidence consistent with a more frequent or persistent glacial throughout much of the Pacific (North Pacific, Western Equatorial Pacific and EEP).

## 1. Introduction

The Pacific Equatorial upwelling system accounts for a substantial proportion (20-50%) of new biological production in the global ocean (Chavez and Barber, 1987) while also being responsible for up to 72% of the oceanic outgassing of CQ to the atmosphere (Feely et al., 1999). Its importance for global climate has led to ongoing interest in the role played by this region during glacial/interglacial cycles (Ford et al., 2018; Keigwin and Lehman, 2015; Lea et al., 2003, 2000; Tudhope et al., 2001; Winckler et al., 2008). One of its important influences on global climate is through the mechanism of perturbations associated with the El Niño - Southern Oscillation (ENSO). El Niño is characterized by an eastward movement of warm surface waters from the western Pacific towards the central Pacific (Clement et al., 2001). This shift results in a lower zonal sea surface temperature gradient across the equatorial Pacific that weakens the Trade Winds, decreases equatorial upwelling and decreases the zonal tilt of the thermocline. These El Niño changes result in extensive perturbations to atmospheric circulation

that synchronously affect climate in widespread regions of the world (Alexander et al., 2002; van Oldenborgh and Burgers, 2005). Swings to the opposite phase (La Niña), with warm water moving back westward, accompanied by associated increases in trade winds, equatorial upwelling and zonal thermocline tilt, lead to a different set of climate changes globally.

ENSO events also have significant effects on atmospheric Colevels. Modern observations have indicated that the net sea to air flux of CO  $_2$  from the equatorial Pacific during an El Niño episode is 30–80% lower than during a non- El Niño year, accounting for up to one third of the atmospheric CO $_2$  anomaly observed during an El Niño period (Feely et al., 1999). Due to ENSO's effect on the carbon cycle, there has been much work in trying to determine the ENSO state of the Last Glacial Maximum (LGM), as the LGM has long been a benchmark for paleoclimate reconstructions and modelling (Otto-Bliesner et al., 2007; Zheng et al., 2008). Despite these efforts, the ENSO state of the tropics during the LGM remains a source of controversy. Several geochemical and modelling studies have indicated an increased El Niño -like state

E-mail address: nivedita@caltech.edu (N. Thiagarajan).

<sup>\*</sup> Corresponding author.

during the LGM (An et al., 2004; Koutavas et al., 2002; Rein et al., 2005), whereas other geochemical and modelling studies have found evidence for a La Niña state (Lea et al., 2000; Martínez et al., 2003; Tudhope et al., 2001) or for no change compared to the modern (Leduc et al., 2009).

Here we focus on one particular aspect of the ENSO system, paleoproductivity in the eastern equatorial Pacific, during the last 30,000 years. During an El Niño phase, the weakening of the trade wind expands the West Pacific warm pool eastward. The deepening of the thermocline in the East Pacific reduces productivity in the east and increases it in the west. The opposite effect is seen during a La Nina (Barber and Chavez, 1983; Rafter et al., 2017). Additionally, ENSO-related perturbations in productivity have also been seen in the North Pacific (Karl et al., 1995) and Southern Ocean (Trathan et al., 2007).

Reconstructing changes in paleoproductivity in the Pacific has been a long-pursued and controversial area of research (Hayes et al., 2011; M. Kienast et al., 2006; Kienast et al., 2013, 2007; S. Kienast et al., 2006; Loveley et al., 2017b; Pichevin et al., 2009; Herguera, 2000). Linear sedimentation rates calculated from core chronologies typically have indicated higher mass accumulation of biogenic material during glacial times, implying higher glacial productivity supporting a La Nina dominated glacial climate (Lyle, 1988; Paytan et al., 1996; Pedersen, 1983; Sarnthein et al., 1988). However constant flux tracers such as  $^{230}\mathrm{Th}$  and  $^{3}\mathrm{He}$  applied during the same glacial time periods have shown that the accumulation of biogenic material in the EEP remained the same during the LGM (18–22 kya) compared to the Holocene (0-11kya) or slightly decreased (Loubere et al., 2004; Marcantonio et al., 2001). The proponents of the constant flux tracers have explained the discrepancy in accumulation rate through changes in sediment redistribution by bottom currents that can influence accumulation rates without affecting stratigraphy or chronology (Francois et al., 2004). We investigate glacial/interglacial productivity in the equatorial Pacific by measuring <sup>231</sup>Pa, <sup>230</sup>Th, <sup>232</sup>Th, <sup>235</sup>U and <sup>238</sup>U at four cores from the Eastern Equatorial Pacific (EEP) (Fig. 1). These cores are located in the core of the modern equatorial Pacific upwelling system and should be sensitive to changes in strength of productivity (Behrenfeld et 2001). We also calculate the <sup>230</sup>Th-normalized fluxes of biogenic and terrigenous material and the <sup>231</sup>Pa to <sup>230</sup>Th excess activity ratio as productivity indicators during this time period (Bacon and Anderson, 1982; Henderson and Anderson, 2003). One particular advantage of

using the ( <sup>231</sup>Pa/<sup>230</sup>Th) ratios is that it is relatively insensitive to remineralization, dilution and sediment redistribution. Finally, we synthesize existing <sup>230</sup>Th-normalized opal fluxes, opal mass accumulation rate records in regions where there are few <sup>230</sup>Th-normalized records (North Pacific) and Pa/Th records to determine changes in productivity across the Pacific during the LGM. In addition, we also place our records, Pa/Th and productivity in particular, into a broader regional context within the Pacific Basin and find a preponderance of evidence consistent with the glacial ocean being more generally in an El Niño state

#### 2. Methods

## 2.1. Equatorial Pacific cores site location

Four cores located along the Equator, KNR73-4 PC (1.84°N 110.27°W 3681 m water depth), KNR73-3 PC (0.37°S 106.18°W 3606 m water depth), VTR01-10 GGC (4.51°S 102.02°W –3405 m water depth) and PLDS-7G (3.39°S 102.45°W 3253 m water depth) were studied (Fig. 1). KNR73 piston cores 3 and 4 were collected in 1978 on R/V Knorr (KNR) cruise 73 by R.P. von Herzen for heat flow studies. PLDS 7G was provided by the curators at Scripps Institute of Oceanography and VNTR01-10 GC was provided by Oregon State University (Keigwin and Lehman, 2015). The cores are all located above the modern carbonate compensation depth and far from terrigenous sources. The dominant sediment at each of the sites was biogenic calcium carbonate.

## 2.2. Age models and stratigraphy

For all cores, we constructed age models based on linear extrapolation between previously published calibrated radiocarbon dates (Keigwin and Lehman, 2015). KNR 73-3 PC had nine  $^{14}\mathrm{C}$  ages from 3.5  $^{14}\mathrm{C}$  ka to 25.8  $^{14}\mathrm{C}$  ka, KNR 73-4 PC had  $^{4}\mathrm{C}$  ages from 5.1  $^{14}\mathrm{C}$  ka to 22.7  $^{14}\mathrm{C}$  ka, VTR01-10 GGC had eight  $^{14}\mathrm{C}$  ages from 12.2  $^{14}\mathrm{Cka}$  to 25.3  $^{14}\mathrm{C}$  ka and PLDS-7G had six  $^{14}\mathrm{C}$  ages from 14.1  $^{14}\mathrm{C}$  ka to 17.4  $^{14}\mathrm{C}$  ka. We used a reservoir age of 450 years and converted the radiocarbon dates to calendar ages using IntCal13 (Table 1).

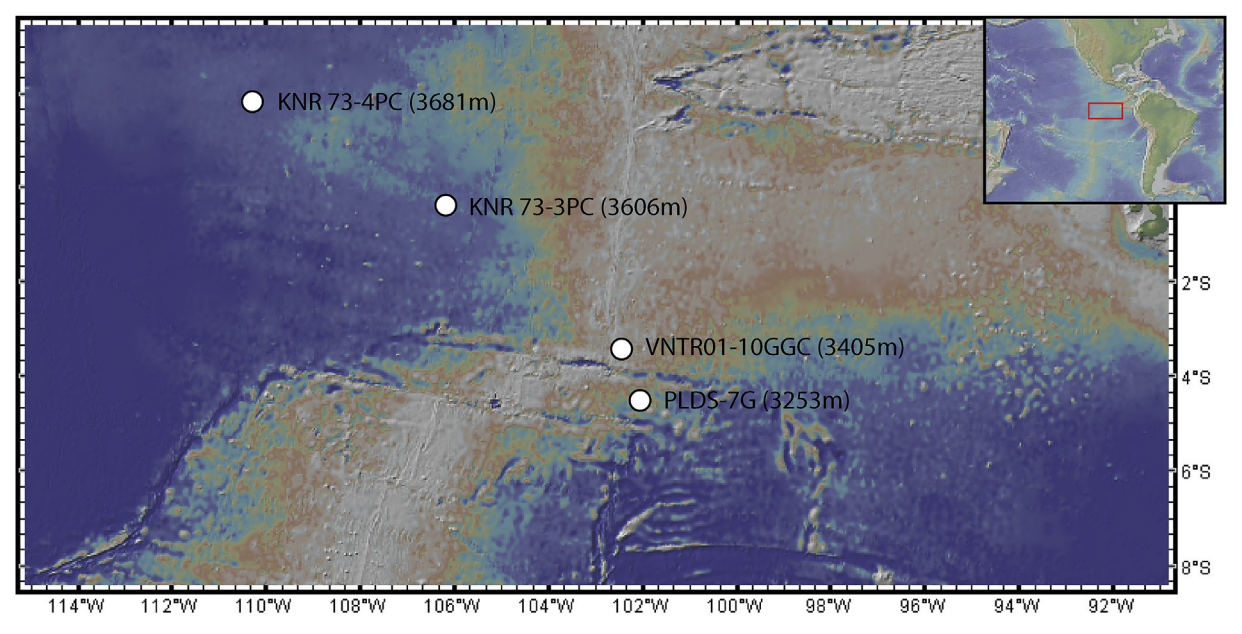


Fig. 1. Core location (white dots): KNR73-4 PC (1.84°N 110.27 °W 3681 m water depth), KNR73-3 PC (0.37°S 106.18°W 3606 m water depth), VTR01-10 GGC (4.51°S 102.02°W –3405 m water depth) and PLDS-7G (3.39 °S 102.45°W 3253 m water depth) in the Eastern Equatorial Pacific.

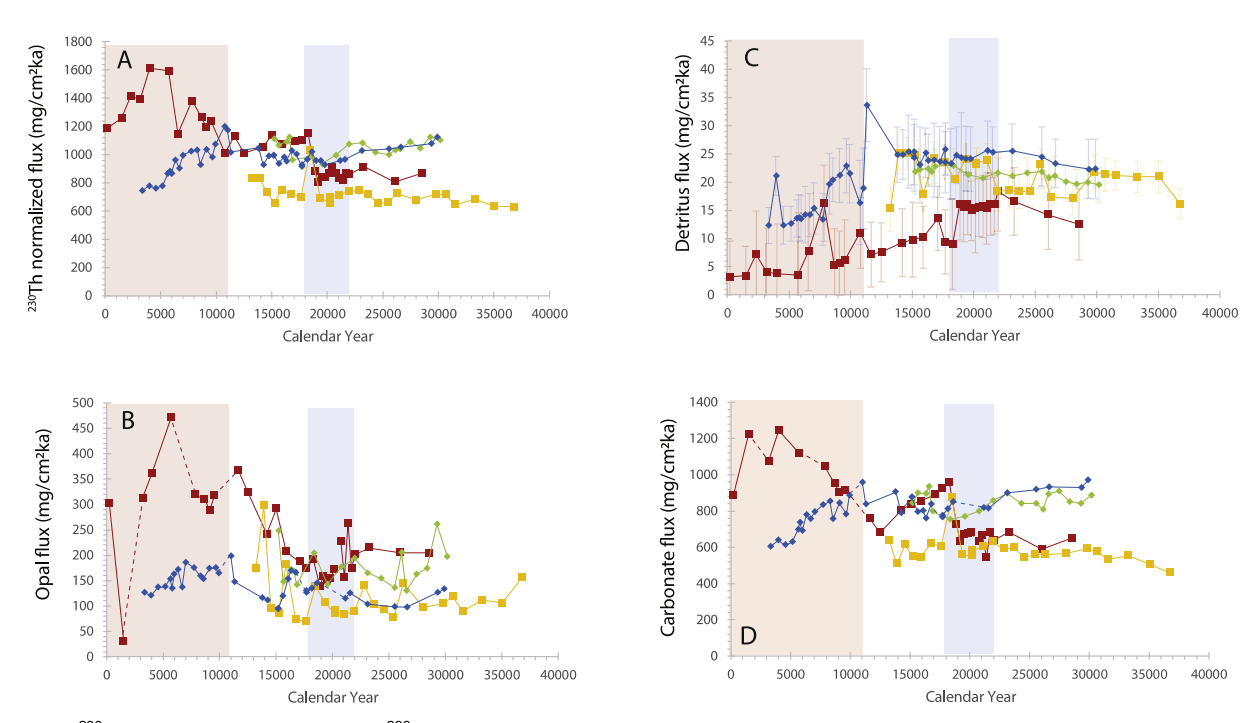


Fig. 2. a-d: The  $^{230}$ Th normalized flux as well as the  $^{230}$ Th-normalized flux of carbonate, opal and detritus in the sediment cores. The LGM and Holocene are shaded in blue and red, respectively. Error bars are  $2\sigma$  and reflect analytical precision.

#### 2.3. Analytical procedures

## 2.3.1. U, Th and Pa analyses

The sediments were spiked and equilibrated with 233Pa and 229Th prior to total dissolution in HNO  $_{3}$ , HF and HClO  $_{4}$ . An aliquot of the solution was spiked with <sup>236</sup>U and <sup>229</sup>Th for direct measurement of <sup>238</sup>U and <sup>232</sup>Th on a single-collector ICP-MS Thermo-Finnigan ELEMENT 2 XR. The remaining solution was used for <sup>231</sup>Pa and <sup>230</sup>Th separation by ion-exchange chromatography and subsequently analyzed on the ELEMENT 2 XR. One hundred and twenty sediment samples were analyzed for U and Th isotopes and 117 samples were analyzed for Pa isotopes (Table 2). Repeated measurements of \$25U/\$238U ratios in the U standard solution NBS960 were used to correct for isotope mass fractionation during ICP-MS analysis. The signal was corrected for instrumental background and blanks linked to chemical procedure and spike addition. The sum of these contributions was always < 0.5% of signal. An internal sediment standard was used for quality control and 6 replicates were run over the course of a year of measurements. These measurements indicate that all isotopes are reproducible with < 5%.

Measurements of <sup>238</sup>U and <sup>232</sup>Th were used to estimate supported, detrital, and ingrown <sup>231</sup>Pa and <sup>230</sup>Th activity. Corrections assuming detrital <sup>238</sup>U/<sup>232</sup>Th ratios of 0.7 (Henderson and Anderson, 2003) were applied to each sample to calculate a range of corrected <sup>231</sup>Pa<sub>xs</sub> and <sup>230</sup>Th<sub>xs</sub> values and their ratios. A detrital <sup>232</sup>Th concentration of 14 ppm (McGee et al., 2016) was used to convert the <sup>232</sup>Th data to a detritus fraction in each analyzed sample. Excess <sup>230</sup>Th values were also corrected for effects of both radioactive decay since deposition and authigenic ingrowth.

## 2.3.2. Calcium carbonate, opal and detrital fraction analyses

Samples were measured for percent calcium carbonate using a coulometer. Detrital fluxes were determined by assuming a fixed  $^{232}\text{Th}$  concentration in sediment. The isotope  $^{232}\text{Th}$  has a relatively narrow range of abundance in the upper continental crust (Rudnick and Gao, 2014). Recent work has determined that  $^{232}\text{Th}$  concentrations in dust is highly size dependent and dust with a grain size of less than 5  $\mu m$  can have a value as high as 14 ppm (McGee et al., 2016). Our cores are located far from continental sources of lithogenic material and we

expect the <sup>232</sup>Th at our site to be delivered predominantly by aeolian processes and thus to have a very small grain size. Therefore, we use a [<sup>232</sup>Th] of 14 ppm to convert our data to bulk detritus. We note that using a lower value of 10.7 ppm (Rudnick and Gao, 2014) would increase the absolute magnitude of the dust flux reconstructed at our study sites but would not alter our interpretation, as the [<sup>232</sup>Th] are very low. After estimating calcium carbonate and detrital content as above, the remaining fraction in each sample was assumed to be opal, as visual inspection reveals negligible contributions from other (e.g., volcanic, extraterrestrial, authigenic) sources.

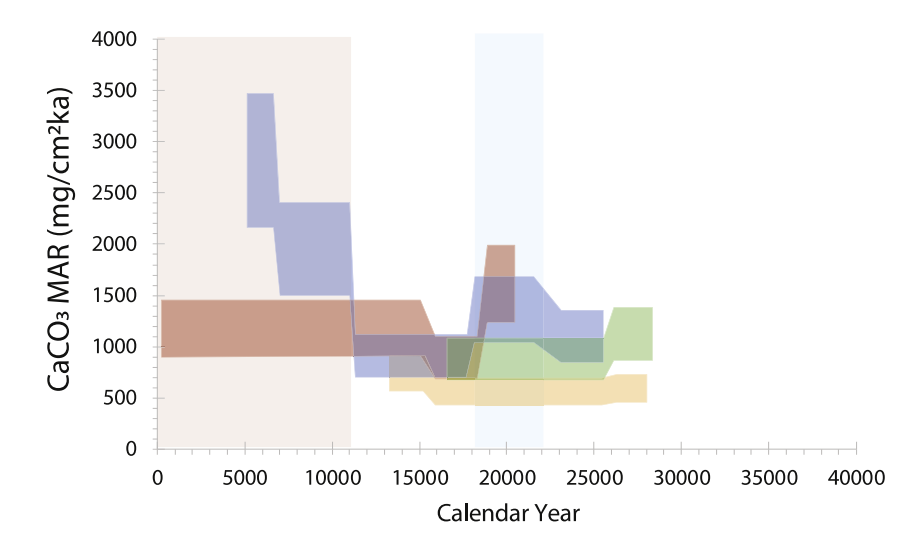
## 3. Results

## 3.1. Mass accumulation rates and Th-normalized fluxes

The calcium carbonate fractions for all cores analyzed were within a range of 70–85%, while the opal fraction within a core ranged from 10 to 30%. For all cores, the detritus fraction was less than 5%, with a tendency for a greater proportion of detritus during the glacial than the Holocene.

We use this data to calculate mass accumulation rates (MAR) based on linear sedimentation rates, and fluxes based on <sup>230</sup>Th normalization. These two approaches are based on different assumptions. MARs based on linear sedimentation rates do not account for the fact that sediments can be redistributed laterally on the seafloor by bottom currents, so that their accumulation may not reflect the vertical rain rate originating from surface and settling through the overlying water column. In contrast, the determination of sedimentary fluxes based on <sup>230</sup>Th normalization is based on the assumption that the rapid scavenging of <sup>230</sup>Th produced in the water column by the constant decay of dissolved uranium results in the <sup>230</sup>Th flux to the seafloor being close to its well-established rate of production. Assuming this is corrected, scavenged <sup>230</sup>Th can be used as a reference to estimate the settling flux of other sedimentary constituents and to correct for sediment redistribution on the seafloor.

The calculated mass accumulation rates (MAR) of calcium carbonate for the four cores ranged from 430 to 3500 mg/cm <sup>2</sup>ka (Fig. 3). The LGM carbonate MARs for all cores range between 430 and 1990 mg/



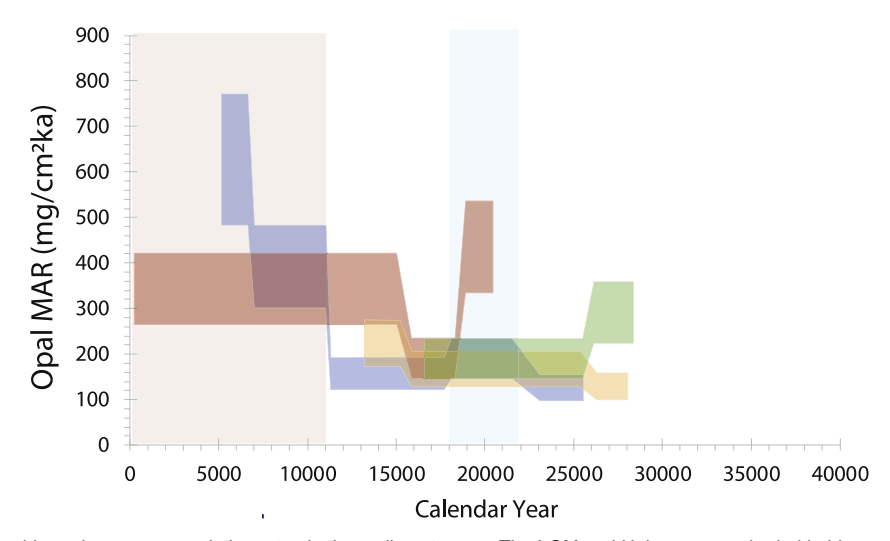


Fig. 3. a-Carbonate and b-opal mass accumulation rates in the sediment cores. The LGM and Holocene are shaded in blue and red, respectively.

cm²ka. The deepest core, KNR73-4 PC has a mid-Holocene increase to 2170–3500 mg/cm ²ka, but otherwise the Holocene carbonate MARs remain between 430 and 1450 mg/cm ²ka. The calculated opal MARs range from 97 to 770 mg/cm ²ka. The cores containing the LGM have opal MAR values of 100–540 mg/cm²ka. The deepest core, KNR73-4 PC has a higher Holocene opal MAR compared to its glacial opal MAR while the shallowest core, PLDS-7G has similar average Holocene and LGM opal MARs.

The total <sup>230</sup>Th-normalized sediment fluxes of the four cores average 960 mg/cm <sup>2</sup>ka (Fig. 2). The opal flux for all four cores is relatively constant through the LGM at 70-270 mg/cm<sup>2</sup>ka. The shallowest core PLDS-7G, shows a marked increase in the opal flux during the Holocene to an average of ~300 mg/cm <sup>2</sup>ka, while the deepest core KNR73-4 PC's Holocene opal flux showed only a small increase compared to the LGM. The detritus fluxes for the three deepest cores are 18–25 mg/cm <sup>2</sup>ka during the LGM. KNR73-4 PC shows a decreased Holocene detritus flux of 16 mg/cm <sup>2</sup>ka compared to the LGM flux. The shallowest core has a lower detrital flux compared to the other cores. Preserved calcium carbonate burial fluxes for all cores are 500-1250 mg/cm<sup>2</sup>ka. During the Holocene, the shallowest core, PLSD7G, has an increased calcium carbonate burial rate, averaging 1010 mg/cm <sup>2</sup>ka compared to average LGM values of 690 mg/cm <sup>2</sup>ka, while the deepest core KNR73-4 PC has a slightly lower preserved burial in the Holocene compared to LGM.

## 3.2. Redox state of cores

Authigenic uranium (aU) deposition may be used to assess the redox conditions prevailing at different locations on and beneath the sea floor. Uranium diffuses from bottom waters and precipitates in suboxic and anoxic sediment pore waters (Mangini et al., 2001). This authigenic fraction of sedimentary U can be estimated by normative calculations using the average <sup>238</sup>U/<sup>232</sup>Th activity ratio of the lithogenic fraction of marine sediments, 0.7 (Henderson and Anderson, 2003). While aU deposition has been shown to vary through time across the tropical Pacific (Jacobel et al., 2017; Pichat et al., 2004) the results here show very little or no aU, thus indicating generally oxidizing conditions, for all cores except the deepest section of the shallowest core, PLDS-7G (Fig. 4).

## 3.3. Variations in $(^{231}Pa/^{230}Th)_{xs}$

All four cores display sedimentary (  $^{231}\text{Pa}/^{230}\text{Th})_{xs}$  that are almost always higher than the water column production ratio of 0.093 (Fig. 5). The Holocene is characterized by higher ( $^{231}\text{Pa}/^{230}\text{Th})_{xs}$  values than the glacial in the shallowest core, PLDS-7G and KNR 73-4 PC.Both cores also show a general trend of increasing values across the deglaciation.

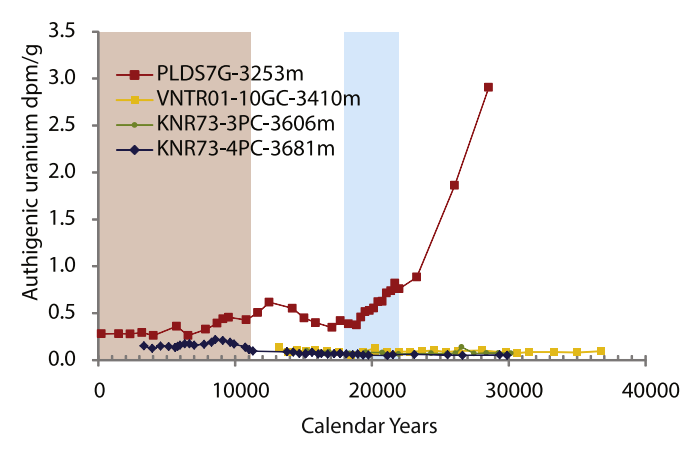


Fig. 4. The authigenic U concentrations for each core. The LGM and Holocene are shaded in blue and red, respectively.

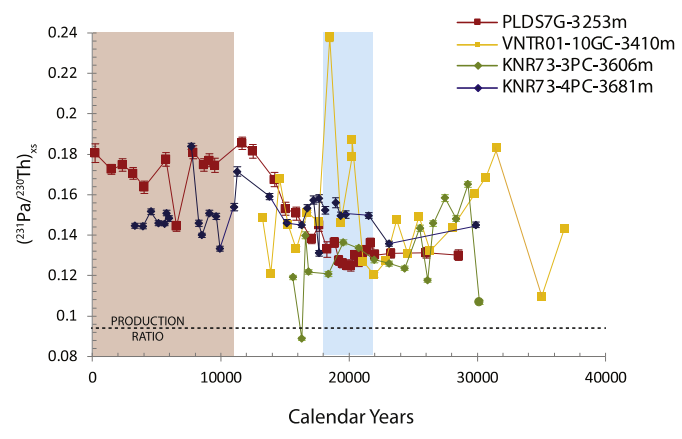


Fig. 5. ( $^{231}$ Pa/ $^{230}$ Th)<sub>xs</sub> for each core. The LGM and Holocene are shaded in blue and red, respectively. Error bars are  $2\sigma$  and reflect analytical precision.

## 3.4. Syndepositional sediment redistribution

Sedimentary  $^{230}$ Th<sub>xs</sub> may be used to assess the extent to which lateral remobilization and redisposition have characterized a given interval of time at a particular site (François et al., 2004). The sediment focusing factor (Suman and Bacon, 1989) has been calculated using the following equation:

$$\Psi = \frac{\int_{r_1}^{r_2} (230 Thxs, o) \rho dr}{\beta z (t_1 - t_2)}$$

where  $r_i$  is the sediment depth in cm,  $t_i$  is the corresponding age deduced from an independent chronology, z is water depth and  $\rho$  is the dry bulk density.  $\Psi > 1$  indicates that more  $^{230} Th_{xs,o}$  has accumulated than produced in the over lying water column, thus indicating a lateral import of sediment to the area while  $\Psi < 1$  indicates a net winnowing. We calculate focusing factors between dated radiocarbon horizons. We find that all cores show relatively low and constant levels of focusing between  $\Psi = 1$  and  $\Psi = 2$ , during the deglaciation, LGM and glacial except for PLDS-7G which shows a small increase to  $\Psi = 3$  at the LGM. Additionally, between 12 and 13.5ka for KNR73-4 PC and 26-30ka for VNTR01-10 GC, both cores show some winnowing (Fig. 6). During the Holocene, focusing factors increase substantially to as high values as  $\Psi = 5$  in the deepest core, KNR73-4 PC, but decrease to 1.7 in the shallowest core, PLDS-7G.

#### 4. Discussion

## 4.1. Influence of particle composition

In the modern Pacific basin, the production and burial of <sup>231</sup>Pa are largely in balance (Haves et al., 2014) so that the spatial pattern of sedimentary  $^{231}\text{Pa}/^{230}\text{Th}_{xs}$  is largely controlled by particle scavenging gradients and the chemical composition of settling particles (Chase et al., 2002; Haves et al., 2014). The presence of MnO2-rich particles as well as the opal/carbonate ratio are thought to affect ( 231Pa/230Th)<sub>xs</sub> values. MnO<sub>2</sub>-rich particles scavenge dissolved<sup>230</sup>Th and <sup>231</sup>Pa with the same efficiency (Anderson et al., 1983a, 1983b), Previous work (Yang et al., 1995) in the Panama Basin has determined that there is a Mn/Al spike centered at the LGM, however ( <sup>231</sup>Pa/<sup>230</sup>Th)<sub>xs</sub> values during the LGM at our sites are lower or unchanged compared to the Holocene, making it unlikely that MnO 2-rich particles are significantly affecting  $(^{231}\text{Pa}/^{230}\text{Th})_{xs}$  values. Opal/carbonate ratios can also play a significant role in affecting ( <sup>231</sup>Pa/<sup>230</sup>Th)<sub>xs</sub> values. In a two-component setting the scavenging of Pa appears to with only these two particle types, increase with increasing opal content and decreasing carbonate content while the affinity of particles for Th increases with increasing carbonate content and decreases with increasing opal content (Chase et al., 2002; Henderson and Anderson, 2003). In the Pacific, it has been shown that sedimentary Pa/Th is largely driven by opal scavenging, suggesting that Pa/Th is a good proxy for diatom productivity (Costa et al., 2016; Hayes et al., 2014).

## 4.2. Authigenic uranium and implications for the redox state of the ocean

Elevated aU levels are only seen in the shallow PLDS-7G core, at a water depth of 3200 m, and not in the deeper cores whose water depths range from 3400 to 3900 m. The precipitation aU is controlled by the combined influence of bottom water oxygen supply and the rate of oxygen consumption as determined by the respiration of organic matter. An increase in the precipitation of aU could be due to a decrease in bottom water oxygen supply, by an increase in respiration due to a larger flux of organic matter from the overlying surface waters, combination of the two. Our <sup>230</sup>Th normalized fluxes of opal indicate that productivity was similar or lower in the glacial compared to the Holocene at these sites, so the higher glacial aU abundance must be due to decreased bottom water oxygen concentrations. Lower bottom water oxygen concentrations suggest that the glacial ocean in this location was oxygen-limited due to increased net respiration and carbon storage associated with decreased rates of ocean ventilation.

The fact that increased aU is only seen in PLDS-7G can be explained by paleo water-mass geometries. In the Pacific there are two main water masses, Antarctic Bottom Water (AABW), which spreads northward into the basin from the Southern Ocean, and North Pacific Deep Water (NPDW), which serves as the return flow southward above the incoming AABW. As a consequence of respiration occurring along the entire flow path and the constant decay of radiocarbon at depth, NPDW is older and less oxygenated while AABW is younger (Key et al., 2004). Radiocarbon data indicates that during the LGM, the water mass below ~3.5 km in the EEP (Keigwin and Lehman, 2015), central equatorial Pacific (Broecker and Clark, 2010), and South Pacific (Gottschalk et al., 2016) was more recently ventilated (younger) than the overlying water mass. Additionally, the high aU values are regionally only seen btwn 2-3.5 km and not in deeper cores (3.8 and 4.5 km), suggesting a similar glacial flow pattern (Jacobel et al., 2017). The combination of the aU data as well as radiocarbon data suggests that during the LGM, there was a floating pool of respired carbon associated with the southward return flow of North Pacific Deep Water, effectively sequestering carbon from the atmosphere into the deep ocean during the Last Glacial Maximum.

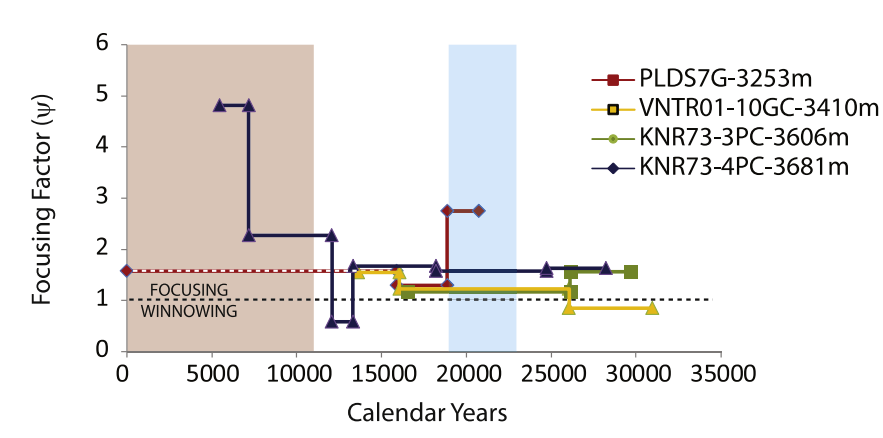


Fig. 6. Focusing factors for each core. Estimates of sediment focusing ( $\Psi$ ) as a result of syndepositional sediment redistribution by bottom currents.  $\Psi$  > 1 indicates focusing while  $\Psi$  < 1 indicates winnowing. The Holocene focusing factor in PLDS 7G is dashed because instead of using  $^{14}C$  measurements to calculate age, we make the focusing factor calculation assuming the top of the sediment core is modern in age.

## 4.3. Implications for paleoproductivity

## 4.3.1. Opal and dust fluxes

Our records allow us to determine paleoproductivity through multiple proxies. The <sup>230</sup>Th-normalized opal flux reconstructions indicate that opal fluxes were relatively low and invariant through the LGM (Fig. 2). The opal flux increased over the deglaciation and Holocene for the shallowest core, PLDS 7G, and more subtly for the deepest core, KNR73-4 PC,indicating that there was less productivity in the glacial compared to the deglaciation and Holocene. This pattern is seen in <sup>230</sup>Th-normalized opal flux and opal MAR reconstructions from elsewhere in the Equatorial Pacific, as well as Southern Ocean and North Pacific (Fig. 7) (Bradtmiller et al., 2006, 2009; Chase et al., 2003; Costa et al., 2016; S. Kienast et al., 2006; Kohfeld and Chase, 2011; Richaud et al., 2007).

Additionally, we calculate <sup>230</sup>Th-normalized dust flux for our records and find that there is an increased dust flux during the glacial compared to the Holocene (Fig. 2). This observation has also been seen previously in the equatorial Pacific and in other major ocean basins

(Costa et al., 2016; Jacobel et al., 2017; McGee et al., 2007; Winckler et al., 2016). Ordinarily an increased dust flux in a major high-nutrient low-chlorophyll region might be associated with increased productivity, especially if the availability of a dust-supplied micronutrient such as iron is otherwise limited (Buesseler et al., 2004; Charette and Buesseler, 2000; Martínez-García et al., 2014). However previous work has shown that although there was an increased dust flux to the glacial Equatorial Pacific, nitrate consumption did not increase (Costa et al., 2016) and productivity was the same or lower. The lack of increased productivity is likely due to the fact that Fe-fertilized productivity in the Subantarctic deprived the Equatorial Pacific of nutrients that would otherwise have been delivered to the Equatorial Pacific via subsurface waters (Costa et al., 2016).

#### 4.3.2. Pa/Th as a paleoproductivity proxy

Pa/Th in marine sediments has multiple controls, including productivity, particle flux, overturning circulation and particle composition. In the Pacific, it has been established that the removal of Pa due to opal scavenging is the strongest control on Pa/Th values, suggesting

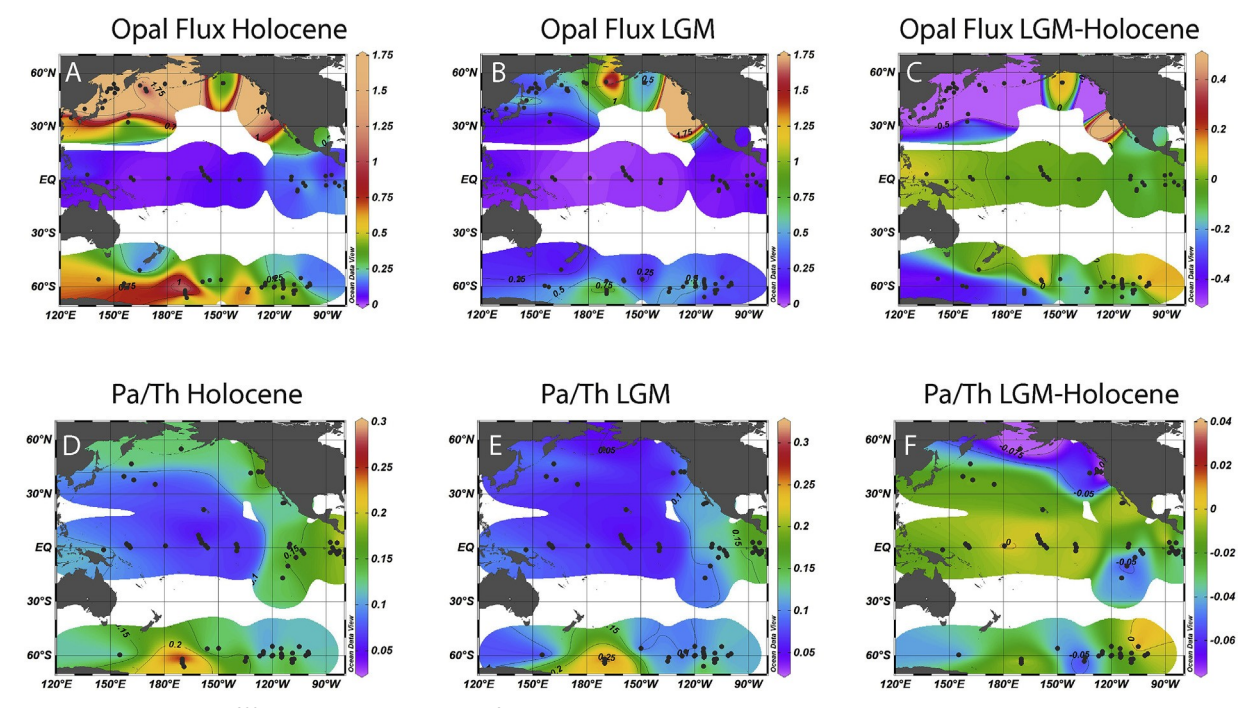


Fig. 7. Compilation of Pacific opal <sup>230</sup>Th normalized fluxes (g/cm <sup>2</sup>kya) (Bradtmiller et al., 2006, 2009; Chase et al., 2003; Costa et al., 2016; S. Kienast et al., 2006; Richaud et al., 2007), opal MARs (Kohfeld and Chase, 2011) and Pa/Th records (Bradtmiller et al., 2006, 2009; Chase et al., 2003; Costa et al., 2016; Dubois et al., 2010; Lao et al., 1992; Pichat et al., 2004; Shimmield and Price, 1988; Yang et al., 1986) during the Holocene (a, d), the LGM (b, e) and the difference between LGM and Holocene (c, f). We see evidence for decreased productivity in the EEP, North Pacific and south of the APF and increased productivity in the Western Equatorial Pacific and parts of the Southern Ocean.

that (  $^{231}$ Pa/ $^{230}$ Th) $_{xs}$  values can be used as a paleoproductivity proxy (Costa et al., 2018a, 2017; 2016; Hayes et al., 2014; Pichat et al., 2004). The ( $^{231}$ Pa/ $^{230}$ Th) $_{xs}$  values for the shallowest core show a similar behavior to  $^{230}$ Th-normalized opal fluxes with low (  $^{231}$ Pa/ $^{230}$ Th) $_{xs}$  values (or productivity) in the glacial and an increase to higher values during the deglaciation and Holocene. The deepest core has a very subtle change in opal flux and similarly does not have a significant change in ( $^{231}$ Pa/ $^{230}$ Th) $_{xs}$  values between the glacial and Holocene.

We use our compilation of Pacific records of Pa/Th with data from both the Holocene and LGM to compare how Pa/Th changed during the last glacial transition (Fig. 7) (Bradtmiller et al., 2006, 2009; Chase et al., 2003, Costa et al., 2016; Dubois et al., 2010; Lao et al., 1992; Pichat et al., 2004. Shimmield and Price, 1988. Yang et al., 1986). There have been more extensive compilations of modern coretop sedimentary Pa/Th records (Hayes et al., 2014; Costa et al., 2018a,b), but here we focus on the difference between the Holocene and LGM. In the Holocene, we find higher than production values in the EEP, Southern Ocean and North Pacific suggesting these regions are net sinks of Pa. In the LGM, sedimentary Pa/Th was lower compared to the Holocene in most areas of the Pacific except the Western Equatorial Pacific and sections of the Southern Ocean. Additionally, only the EEP and Southern Ocean have elevated Pa/Th values above production, gesting that Pa removal was not as widespread in the LGM ocean compared to the Holocene. However, there are vast regions of the Pacific where we have limited LGM data, for instance the subarctic Pacific, which in the modern ocean is a major sink for Pa (Hayes et al., 2014). Future mapping of LGM sediments will be required to evaluate the extent of the sink of Pa in the Pacific LGM ocean.

## 4.4. Focusing factors

Sediment redistribution and focusing in the equatorial Pacific have been the subjects of considerable debate in recent years (Bista et al., 2016; Broecker, 2008; François et al., 2007; Loveley et al., 2017a; Lyle et al., 2005, 2007; 2014; Marcantonio et al., 2001; Singh et al., 2011). Paleoproductivity estimates derived by MARs and 230Th normalized fluxes are sometimes widely discrepant, notably in the EEP, where MARs indicate higher fluxes during the last glacial period compared to Holocene fluxes (Herguera and Berger, 1991; Lyle et al., 2005; Paytan et al., 1996) while <sup>230</sup>Th normalization indicates unchanged or lower glacial fluxes compared to Holocene fluxes (Anderson et al., 2006; Bradtmiller et al., 2009; Costa et al., 2017; Pichat et al., 2004). This discrepancy has been attributed by the latter group to enhanced glacial sediment focusing near the equator, resulting in greater local accumulation of productivity proxies that had settled vertically over a broader area of ocean (Francois et al., 2007; Loubere et al., 2004; Marcantonio et al., 2001). However, this interpretation has been disputed (Lyle et al., <sup>230</sup>Th normalization grossly over-2005), with the contention that estimates sediment focusing in the equatorial Pacific and that lateral transport of <sup>230</sup>Th in the water is much larger than generally appreciated. Indeed there has been recent evidence for lateral near-bottom <sup>230</sup>Th transport in the bottom nepheloid layer in the equatorial Pacific (Lyle et al., 2014). The frequent disagreement of these approaches raises the question of which conclusion regarding glacial productivity they would reach in settings where estimates based on the two methods might agree. Our study offers at least one such setting, where focusing of glacial sediment is not a potentially confounding overprint. deepest core, KNR-73 4 PC, where we have focusing factors, calculated MARs and <sup>230</sup>Th normalized fluxes for the glacial and Holocene, we find that focusing is higher in the Holocene compared to glacial, indicating neither enhanced deposition of laterally transported glacial sediment (Francois et al., 2007; Loubere et al., 2004; Marcantonio et al., 2001), nor preferential glacial scavenging of laterally transported seawater Th (Lyle et al., 2005, 2014). At this location the calcium carbonate MAR, opal MAR and <sup>230</sup>Th normalized opal flux are all higher in the Holocene than glacial. This finding supports recently emerging evidence form the

Pacific for lower glacial productivity (Costa et al., 2017, 2016; Pichat et al., 2004). We do find that in the deepest core the <sup>230</sup>Th normalized calcium carbonate flux is lower in the Holocene than the glacial, but do not interpret this feature as indicative of increased glacial productivity because the decreased Holocene calcium carbonate flux is most likely due to dissolution from a shallower lysocline (Farrell and Prell, 1989), overriding any existing productivity signal. In the shallowest core, PLDS-7G, we do not have a radiocarbon date in the Holocene. However, if we assume that the core top is modern, then we can calculate a focusing factor for the Holocene. We find a subtly different pattern in MAR and <sup>230</sup>Th normalized fluxes compared to the deepest core. Both the carbonate and opal MAR are higher in the glacial compared to Holocene while the <sup>230</sup>Th normalized fluxes are higher in the Holocene compared to glacial. Previous work has suggested that discrepant MARs and <sup>230</sup>Th-normalized fluxes can be explained by increased focusing and indeed our calculated focusing factors show higher levels of cusing in the glacial compared to the Holocene. In summary, at our site where the MAR and <sup>230</sup>Th-normalized approaches agree and there is negligible lateral focusing, glacial productivity is lower, whereas at the site where the two methods disagree, the <sup>230</sup>Th-normalized approach also indicates lower glacial productivity and the MAR appears to be influenced by enhanced glacial focusing.

## 4.5. Implications for ENSO state of LGM

During an El Niño event, there are strong changes in productivity in the Equatorial Pacific, with decreased productivity in the EEP and increased productivity in the Western Equatorial Warm Pool (Barber and Chavez, 1983; Messié and Chavez, 2012). Analyses of modern ENSO indicates that during El Niños there is also reduced productivity in the Arabian Sea, Western Bay of Bengal and central North Pacific (between 50 and 70 °N), and increased productivity in the Western Equatorial Pacific, Southern Ocean and central North Pacific (between 15 and 30°N and less strongly 50-60 °N) (see Fig. 6h in (Messié and Chavez, 2012). Here we use our records and place them within the context of a synthesis of previously published Pa/Th and opal records (MARs and 230 Th normalized) in the Pacific to investigate if basin wide changes in productivity are consistent with a more frequent or persistent El Niño or La Niña state in the LGM (Fig. 7).

As noted above, we find evidence via decreased  $^{230}\text{Th}$  normalized opal fluxes and Pa/Th ratios for generally reduced productivity in the EEP during the LGM. These results are consistent with more EI Niño-like conditions during the late glacial. Evidence for a glacial EI Niño-like state in the EEP is also supported by previous studies of Mg/Ca and  $\delta^{18}\text{O}$  measurements in foraminifera examining zonal temperature gradients across the EEP during the LGM (Ford et al., 2018, 2015; Koutavas et al., 2002; Koutavas and Joanides, 2012; Stott et al., 2002). During the glacial interval, there appears to have been a deepened thermocline in the EEP (Ford et al., 2018), either through increased frequency of El Niño events or a more persistent mean pattern more similar to El Niño conditions. A deepened thermocline reduces the nutrient supply to the surface waters as nutrient-rich waters are trapped below the depth from which upwelled waters are drawn.

In our compilation of previously published records, we also find broad evidence for decreased productivity in the North Pacific between 30 and 50 °N (Costa et al., 2018b; Messié and Chavez, 2012) and increased productivity in the Western Equatorial Pacific (Bradtmiller et al., 2006), both of which are consistent with an El Niño state (Fig. 7). However, the Southern Ocean has a productivity distribution both in opal and Pa/Th records different than the increase expected from modern ENSO analyses (Messié and Chavez, 2012). Glacial productivity in the Pacific sector of the Southern Ocean is lower south of the Antarctic Polar Front (APF) but shows little to no change north of the APF. Future work could clarify whether the increased presence of Southern Ocean sea ice during the LGM changed the expected biological responses of increased Southern Ocean productivity (as suggested by

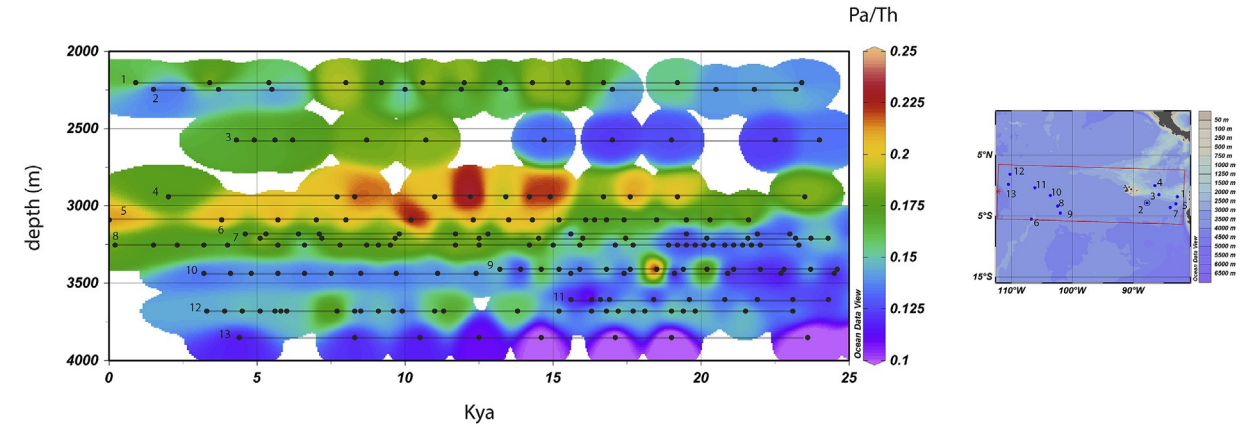


Fig. 8. A compilation of Pa/Th records near the East Pacific Rise. The numbers of the cores correspond to the following names and publications: Core 1-ME0005-27JC, Core 4-ME 0005-24JC, Core 7-TR163-31 (Dubois et al., 2010), Core 2-RC13-140, Core 3-RC11-238, Core 5-V19-30, Core 6-V21-40, Core 10-RC13-114 (Bradtmiller et al., 2006), Core 13-ODP 849 (Pichat et al., 2004) and Core 8-PLDS 7G, Core 9-VTR01-10 GGC, Core 11-KNR73-3 PC, Core 12-KNR73-4 PC (present study). We find increased Pa/Th values near the tops of MORs. However these cores (4–8 and 12) are all also associated with increased opal fluxes, making the effects of increased scavenging due to increased hydrothermal activity and increased productivity difficult to disentangle.

Messié and Chavez, 2012) during El Niño events. We note that this scenario of decreased productivity poleward of the APF has been seen before and is attributed to increased sea ice south of the APF limiting consumption of upwelled Si which is in turn transported northward (Chase et al., 2003).

Despite evidence consistent with El Niño in the EEP, WEP and central N Pacific, our data cannot conclusively confirm an El Niño-like state for the LGM for two reasons. The first is that the Southern Ocean has a signature distinct from what is expected from modern El Niño analyses. Second, the decreased productivity seen in the EEP could be due to changes in the source region for the upwelled water in the EEP. Indeed there is evidence for lower glacial nitrate concentrations exported in Sub Antarctic Mode Water to the low latitudes (Costa et al., 2016; Robinson et al., 2005; Sarmiento et al., 2004). Therefore, although regions of the LGM Pacific are consistent with a more El Niño-like state of the Pacific Ocean, we cannot uniquely conclude that there was a glacial El Niño configuration.

#### 4.6. Pa/Th ratios near mid ocean ridges

Late Pleistocene glacial cycles are characterized by changes in atmospheric CO<sub>2</sub> (Petit et al., 1999) that change nearly in phase with Antarctic temperature (Pedro et al., 2011), suggesting that CO<sub>2</sub> is the trigger for initiating glaciations. Despite CO<sub>2</sub>'s central role in glacial/ interglacial cycles, the causes for the CO 2 changes are not well understood. Atmospheric CO<sub>2</sub> increased by ~80 ppm during the last several deglaciations, and most hypotheses seeking to explain this phenomenon invoke the release of CO2 from the Southern Ocean back to the atmosphere (Anderson et al., 2009; Burke and Robinson, 2012; Marchitto et al., 2007; Sigman and Boyle, 2000; Sigman et al., 2010). However, surface to mid depth radiocarbon profiles are not significantly different in the Pacific during the LGM and Holocene (Lund, 2013), the deep Pacific carbonate ion concentration does not change significantly over the last glacial cycle (Yu et al., 2013) and there is no widespread excess in preservation of calcium carbonate in the deep-sea during the deglaciation (Mekik et al., 2012) as should accompany a substantial rapid outgassing of CO<sub>2</sub> (Broecker and Peng, 1987). An alternate hypothesis is that variations in volcanic CO 2 emissions contribute to glacial/interglacial CO<sub>2</sub> variations (Huybers and Langmuir, 2017; Lund et al., 2016).

Although our study was not designed to look for effects of enhanced hydrothermal activity during the deglaciation, our compilation of Pa/Th data includes records near the mid-ocean ridge (MOR) system in the Pacific, and Pa/Th records are sensitive to Mn-oxides produced by

hydrothermal activity (Anderson et al., 1983a, 1983b; Lund et al., 2019). We find that superimposed upon a broad glacial to Holocene increase in Pa/Th, records near the depth of the tops of MORs show elevated Pa/Th ratios in the deglaciation (Fig. 8). At first glance, this correlation seems to be evidence of Pa/Th responding to enhanced hydrothermal activity during the deglaciation. However, in each of the records increased Pa/Th (records 4–8 and 12) is tightly correlated with increased <sup>230</sup>Th-normalized opal fluxes (Costa et al., 2017; Dubois et al., 2010; present study). This simultaneous correspondence of increased Pa/Th with increased hydrothermal activity and greater opal flux makes the effect of increased scavenging due to opal flux and Mnoxides difficult to disentangle. Future work will entail measuring Fe oxyhydroxides and Mnoxides in the core to separate the effect of increased hydrothermal activity in the East Pacific Rise and productivity on these Pa/Th records.

#### 5. Conclusions

We have determined paleoproductivity at sites in the EEP for the past 30,000 years using multiple proxies and find significant evidence for lower productivity in the glacial interval compared to the Holocene based on sedimentary (  $^{231}$ Pa/ $^{230}$ Th)<sub>xs</sub>, along with  $^{230}$ Th-normalized fluxes of calcium carbonate and opal. We also see possible features of CaCQ dissolution in the Holocene section of the deeper cores, reflected in reduced  $^{230}$ Th-normalized burial fluxes of calcium carbonate (KNR 73-4 PC) in the Holocene compared to the glacial interval.

Previous records indicating greater glacial productivity in the EEP using MARs have been attributed to higher lateral sediment focusing during that time. Here we examine two different cores in the EEP, one where calculated focusing factors are relatively low during the glacial and then increase into the Holocene, and another with higher focusing in the glacial and lower focusing in the Holocene. In the first of these cores, KNR 73-4 PC, where focusing is lower in the glacial than Holocene, both the MARs and the <sup>230</sup>Th-normalized fluxes indicate lower glacial productivity as compared to the Holocene. This finding is in contrast to the second core, PLDS-7G, which has the highest focusing overall, with higher focusing in the glacial compared to the Holocene, and is characterized by higher glacial MARs but lower glacial <sup>230</sup>Thnormalized fluxes. These observations support findings that MAR records showing an increased glacial productivity in the EEP are more likely to be biased by increased glacial sediment focusing.

We put our productivity and Pa/Th records in the context of other records from the Pacific and find evidence for decreased productivity throughout the EEP and North Pacific, along with increased

productivity in the WEP, all of which are consistent with a generally more El Niño like state of the Pacific during the glacial interval. However, the Southern Ocean's productivity signature is discrepant from modern El Niño productivity distributions. Therefore, although large regions of the Pacific display evidence that is consistent with a more El Niño like state, we cannot unequivocally confirm a glacial El Niño configuration.

Finally, we examine Pa/Th records near the East Pacific Rise where increased hydrothermal activity has been shown to have occurred during the deglaciation. We find that superimposed on the broad glacial to interglacial increase in Pa/Th there is a deglacial spike in Pa/Th at mid depths. This increase could be due to a deglacial increase in productivity (Hayes et al., 2011) or related to increased hydrothermal activity (Lund et al., 2016). Future work such as measurements of Fe, Mn and other proxies sensitive to hydrothermal activity will be required to constrain the potential effect of hydrothermal activity on Pa/Th during the deglaciation at the East Pacific Rise.

#### Acknowledgements

We thank Martin Fleisher at LDEO for assistance with sample analysis, Ellen Roosen for assistance at the WHOI core repository, and Lloyd Keigwin for samples, data, and discussions. This work was supported in part by the National Science Foundation awards OCE-1029936 and OCE-1835997 to JFM.

## Appendix A. Supplementary data

Supplementary data to this article can be found online at https://doi.org/10.1016/j.dsr.2019.03.007

#### References

- Alexander, M.A., Bladé, I., Newman, M., Lanzante, J.R., Lau, N.-C., Scott, J.D., 2002. The atmospheric bridge: the influence of ENSO teleconnections on air–sea interaction over the global oceans. J. Clim. 15, 2205–2231. https://doi.org/10.1175/1520-0442/2002)015
- An, S.I., Timmermann, A., Bejarano, L., Jin, F.F., Justino, F., Liu, Z., Tudhope, A.W., 2004. Modeling evidence for enhanced El Niño–southern oscillation amplitude during the last glacial maximum. Paleoceanography 19, PA4009. https://doi.org/10.1029/ 2004PA001020.
- Anderson, R.F., Ali, S., Bradtmiller, L.I., Nielsen, S.H.H., Fleisher, M.Q., Anderson, B.E., Burckle, L.H., 2009. Wind-driven upwelling in the Southern Ocean and the deglacial rise in atmospheric CO2. Science 323, 1443–1448. https://doi.org/10.1126/science. 1167441.
- Anderson, R.F., Bacon, M.P., Brewer, P.G., 1983a. Removal of Th-230 and Pa-231 from the open ocean. Earth Planet. Sci. Lett. 62, 7–23.
- Anderson, R.F., Bacon, M.P., Brewer, P.G., 1983b. Removal of Th-230 and Pa-231 at ocean margins. Earth Planet. Sci. Lett. 66, 73–90.
- Anderson, R.F., Fleisher, M.Q., Lao, Y., 2006. Glacial-interglacial variability in the delivery of dust to the central equatorial Pacific Ocean. Earth Planet. Sci. Lett. 242, 406–414. https://doi.org/10.1016/j.epsl.2005.11.061.
- Bacon, M.P., Anderson, R.F., 1982. Distribution of Thorium isotopes between dissolved and particulate forms in the deep sea. J. Geophys. Res. 87, 2045–2056.
- Barber, R.T., Chavez, F.P., 1983. Biological consequences of El Niño. Science 222, 1203–1210.
- Behrenfeld, M.J., Randerson, J.T., McClain, C.R., Feldman, G.C., Los, S.O., Tucker, C.J., Falkowski, P.G., Field, C.B., Frouin, R., Esaias, W.E., Kolber, D.D., Pollack, N.H., 2001. Biospheric primary production during an ENSO transition. Science 291, 2594. https://doi.org/10.1126/science.1055071.
- Bista, D., Kienast, S.S., Hill, P.S., Kienast, M., 2016. Sediment sorting and focusing in the eastern equatorial Pacific. Mar. Geol. 382, 151–161. https://doi.org/10.1016/j. margeo.2016.09.016.
- Bradtmiller, L.I., Anderson, R.F., Fleisher, M.Q., Burckle, L.H., 2009. Comparing glacial and Holocene opal fluxes in the pacific sector of the Southern Ocean. Paleoceanography 24, PA2214. https://doi.org/10.1029/2008PA001693.
- Bradtmiller, L.I., Anderson, R.F., Fleisher, M.Q., Burckle, L.H., 2006. Diatom productivity in the equatorial Pacific Ocean from the last glacial period to the present: a test of the silicic acid leakage hypothesis. Paleoceanography 21, PA4201. https://doi.org/10.1029/2006pa001282.
- Broecker, W., 2008. Excess sediment 230Th: transport along the sea floor or enhanced water column scavenging? Glob. Biogeochem. Cycles 22, GB1006. https://doi.org/ 10.1029/2007GB003057.
- Broecker and Peng, 1987. The role of CaCO3 compensation in the glacial to interglacial atmospheric CO2 change. Glob. Biogeochem. Cycles 1 (1), 15–29 Biogeochem.

- Cycles. 1(1).
- Broecker, W., Clark, E., 2010. Search for a glacial-age 14C-depleted ocean reservoir. Geophys. Res. Lett. 37. https://doi.org/10.1029/2010GL043969.
- Buesseler, K.O., Andrews, J.E., Pike, S.M., Charette, M.A., 2004. The effects of iron fertilization on carbon sequestration in the Southern Ocean. Science 304, 414–417. https://doi.org/10.1126/science.1086895.
- Burke, A., Robinson, L.F., 2012. The Southern Ocean's role in carbon exchange during the last deglaciation. Science 335, 557–561. https://doi.org/10.1126/science.1208163.
- Charette, M.A., Buesseler, K.O., 2000. Does iron fertilization lead to rapid carbon export in the Southern Ocean? Geochem. Geophys. Geosyst. 1, 2000GC000069.
- Chase, Z., Anderson, R., Fleisher, M.Q., Kubik, P.W., 2002. The influence of particle composition and particle flux on scavenging of Th, Pa and Be in the ocean. Earth Planet. Sci. Lett. 204, 215–229.
- Chase, Z., Anderson, R.F., Fleisher, M.Q., Kubik, P.W., 2003. Accumulation of biogenic and lithogenic material in the Pacific sector of the Southern Ocean during the past 40,000 years. Deep Sea Res. Part II Top. Stud. Oceanogr. 50, 799–832. https://doi. org/10.1016/S0967-0645(02)00595-7.
- Chavez, F.P., Barber, R.T., 1987. An estimate of new production in the equatorial Pacific. Deep Sea Research Part A. Oceanogr. Res. Pap. 34, 1229–1243. https://doi.org/10.1016/0198-0149(87)90073-2.
- Clement, A.C., Cane, M.A., Seager, R., 2001. An orbitally driven tropical source for abrupt climate change. J. Clim. 14, 2369–2375.
- Costa, K.M., Anderson, R.F., McManus, J.F., Winckler, G., Middleton, J.L., Langmuir, C.H., 2018a. Trace element (Mn, Zn, Ni, V) and authigenic uranium (aU) geochemistry reveal sedimentary redox history on the Juan de Fuca Ridge, North Pacific Ocean. Geochem. Cosmochim. Acta 236, 79–98. https://doi.org/10.1016/j.gca.2018.02.016.
- Costa, K.M., Jacobel, A.W., McManus, J.F., Anderson, R.F., Winckler, G., Thiagarajan, N., 2017. Productivity patterns in the equatorial Pacific over the last 30,000 years. Glob. Biogeochem. Cycles 31, 2016GB005579. https://doi.org/10.1002/2016GB005579.
- Costa, K.M., McManus, J.F., Anderson, R.F., 2018b. Paleoproductivity and stratification across the subarctic pacific over glacial-interglacial cycles. Paleoceanogr. Paleoclimatol. 33, 914–933. https://doi.org/10.1029/2018PA003363.
- Costa, K.M., McManus, J.F., Anderson, R.F., Ren, H., Sigman, D.M., Winckler, G., Fleisher, M.Q., Marcantonio, F., Ravelo, A.C., 2016. No iron fertilization in the equatorial Pacific Ocean during the last ice age. Nature 529, 519–522. https://doi.org/10.1038/nature16453.
- Dubois, N., Kienast, M., Kienast, S., Calvert, S., François, R., Anderson, R., 2010.
  Sedimentary opal records in the eastern equatorial Pacific: it is not all about leakage.
  Glob. Biogeochem. Cycles 24. https://doi.org/10.1029/2010GB003821
- Farrell, J.W., Prell, W.L., 1989. Climatic change and CaCO3 preservation: an 800,000 Year bathymetric reconstruction from the central equatorial Pacific Ocean. Paleoceanography 4, 447–466. https://doi.org/10.1029/PA004i004p00447.
- Feely, R.A., Wanninkhof, R., Takahashi, T., Tans, P., 1999. Influence of El Niño on the equatorial Pacific contribution to atmospheric CO2 accumulation. Nature 398, 597.
- Ford, H.L., McChesney, C.L., Hertzberg, J.E., McManus, J.F., 2018. A deep eastern equatorial pacific thermocline during the last glacial maximum. Geophys. Res. Lett. 45 (11), 806–811. 816. https://doi.org/10.1029/2018GL079710.
   Ford, H.L., Ravelo, A.C., Polissar, P.J., 2015. Reduced El Niño–southern oscillation during
- Ford, H.L., Ravelo, A.C., Polissar, P.J., 2015. Reduced El Niño-southern oscillation during the last glacial maximum. Science 347, 255. https://doi.org/10.1126/science. 1258437
- Francois, R., Frank, M., Rutgers van der Loeff, M., Bacon, M., 2004. 230Th normalization: an essential tool for interpreting sedimentary fluxes during the late Quaternary. Paleoceanography 19. https://doi.org/10.1029/2003PA000939.
- Francois, R., Frank, M., Rutgers van der Loeff, M., Bacon, M.P., Geibert, W., Kienast, S., Anderson, R.F., Bradtmiller, L., Chase, Z., Henderson, G., Marcantonio, F., Allen, S.E., 2007. Comment on "Do geochemical estimates of sediment focusing pass the sediment test in the equatorial Pacific?" by M. Lyle et al. Paleoceanography 22, PA1216. https://doi.org/10.1029/2005PA001235.
- Gottschalk, J., Skinner, L.C., Lippold, J., Vogel, H., Frank, N., Jaccard, S.L., Waelbroeck, C., 2016. Biological and physical controls in the Southern Ocean on past millennial-scale atmospheric CO2 changes. Nat. Commun. 7, 11539.
- Hayes, C., Anderson, R., Fleisher, M.Q., 2011. Opal accumulation rates in the equatorial Pacific and mechanisms of deglaciation. Paleoceanography 26. https://doi.org/10. 1029/2010PA002008
- Hayes, C.T., Anderson, R.F., Fleisher, M.Q., Serno, S., Winckler, G., Gersonde, R., 2014. Biogeography in 231Pa/230Th ratios and a balanced 231Pa budget for the Pacific Ocean. Earth Planet. Sci. Lett. 391, 307–318. https://doi.org/10.1016/j.epsl.2014. 02.001
- Henderson, G.M., Anderson, R.F., 2003. The U-series toolbox for paleoceanography. Rev. Mineral. Geochem. 52, 493–531. https://doi.org/10.2113/0520493.
- Herguera, J.C., 2000. Last glacial paleoproductivity patterns in the eastern equatorial Pacific: benthic foraminifera records. Mar. Micropaleontol. 40, 259–275. https://doi. org/10.1016/S0377-8398(00)00041-4.
- Herguera, J.C., Berger, W.H., 1991. Paleoproductivity from benthic foraminifera abundance: glacial to postglacial change in the west-equatorial Pacific. Geology 19, 1173–1176. https://doi.org/10.1130/0091-7613(1991)019<1173:pfbfag>2.3.co;2.
- Huybers, P., Langmuir, C.H., 2017. Delayed CO2 emissions from mid-ocean ridge volcanism as a possible cause of late-Pleistocene glacial cycles. Earth Planet. Sci. Lett. 457, 238–249. https://doi.org/10.1016/j.epsl.2016.09.021.
- Jacobel, A.W., McManus, J.F., Anderson, R.F., Winckler, G., 2017. Repeated storage of respired carbon in the equatorial Pacific Ocean over the last three glacial cycles. Nat. Commun. 8, 1727. https://doi.org/10.1038/s41467-017-01938-x.
- Karl, D.M., Letelier, R., Hebel, D., Tupas, L., Dore, J., Christian, J., Winn, C., 1995. Ecosystem changes in the North pacific subtropical gyre attributed to the 1991–92 El Niño. Nature 373, 230.

- Keigwin, L.D., Lehman, S.J., 2015. Radiocarbon evidence for a possible abyssal front near 3.1 km in the glacial equatorial Pacific Ocean. Earth Planet. Sci. Lett. 425, 93–104. https://doi.org/10.1016/j.epsl.2015.05.025.
- Key, R.M., Kozyr, A., Sabine, C.L., Lee, K., Wanninkhof, R., Bullister, J.L., Feely, R.A., Millero, F.J., Mordy, C., Peng, T.-H., 2004. A global ocean carbon climatology: results from global data analysis project (GLODAP). Glob. Biogeochem. Cycles 18. https:// doi.org/10.1029/2004GB002247.
- Kienast, M., Kienast, S.S., Calvert, S.E., Eglinton, T.I., Mollenhauer, G., François, R., Mix, A.C., 2006a. Eastern Pacific cooling and Atlantic overturning circulation during the last deglaciation. Nature 443, 846.
- Kienast, S., Kienast, M., Jaccard, S., Calvert, S.E., François, R., 2006b. Testing the silica leakage hypothesis with sedimentary opal records from the eastern equatorial Pacific over the last 150 kyrs. Geophys. Res. Lett. 33. https://doi.org/10.1029/ 2006GI 026651
- Kienast, S., Friedrich, Tobias, Dubois, Nathalie, Hill, Paul S., Timmermann, Axel, Mix, Alan C., Kienast, Markus, 2013. Near collapse of the meridional SST gradient in the eastern equatorial Pacific during Heinrich Stadial 1. Paleoceanography 28, 663–674. https://doi.org/10.1002/2013PA002499.
- Kienast, S., Kienast, M., Mix, A.C., Calvert, S.E., François, R., 2007. Thorium-230 normalized particle flux and sediment focusing in the Panama Basin region during the last 30,000 years. Paleoceanography 22, PA2213. https://doi.org/10.1029/2006pa001357
- Kohfeld, K.E., Chase, Z., 2011. Controls on deglacial changes in biogenic fluxes in the North Pacific Ocean. Quat. Sci. Rev. 30, 3350–3363. https://doi.org/10.1016/j. quascirev.2011.08.007.
- Koutavas, A., Joanides, S., 2012. El Niño–southern oscillation extrema in the Holocene and last glacial maximum. Paleoceanography 27. https://doi.org/10.1029/ 2012PA002378.
- Koutavas, A., Lynch-Stieglitz, J., Marchitto, T., Sachs, J., 2002. El Nino-like pattern in ice age tropical Pacific sea surface temperature. Science 297, 226–230.
- Lao, Y., Anderson, R.F., Broecker, W.S., 1992. Boundary scavenging and deep-sea sediment dating: constraints from excess 230Th and 231Pa. Paleoceanography 7, 783–798. https://doi.org/10.1029/92PA02042.
- Lea, D.W., Pak, D., Peterson, L.C., Hughen, K., 2003. Synchroneity of tropical and highlatitude atlantic temperatures over the last glacial maximum. Science 301, 1361–1364.
- Lea, D.W., Pak, D.K., Spero, H.J., 2000. Climate impact of late Quaternary equatorial Pacific sea surface temperature variations. Science 289, 1719–1724.
- Leduc, G., Vidal, L., Cartapanis, O., Bard, E., 2009. Modes of eastern equatorial Pacific thermocline variability: implications for ENSO dynamics over the last glacial period. Paleoceanography 24, PA3202. https://doi.org/10.1029/2008PA001701.
- Loubere, P., Mekik, F., Francois, R., Pichat, S., 2004. Export fluxes of calcite in the eastern equatorial Pacific from the Last Glacial Maximum to present. Paleoceanography 19, PA2018. https://doi.org/10.1029/2003pa000986.
- Loveley, M.R., Marcantonio, F., Lyle, M., İbrahim, R., Hertzberg, J.E., Schmidt, M.W., 2017a. Sediment redistribution and grainsize effects on 230Th-normalized mass accumulation rates and focusing factors in the Panama Basin. Earth Planet. Sci. Lett. 480, 107–120. https://doi.org/10.1016/j.epsl.2017.09.046.
- Loveley, M.R., Marcantonio, F., Wisler, M.M., Hertzberg, J.E., Schmidt, M.W., Lyle, M., 2017b. Millennial-scale iron fertilization of the eastern equatorial Pacific over the past 100,000 years. Nat. Geosci. 10, 760.
- Lund, D.C., 2013. Deep Pacific ventilation ages during the last deglaciation: evaluating the influence of diffusive mixing and source region reservoir age. Earth Planet. Sci. Lett. 381, 52–62. https://doi.org/10.1016/j.epsl.2013.08.032.Lund, D.C., Asimow, P.D., Farley, K.A., Rooney, T.O., Seeley, E., Jackson, E.W., Durham,
- Lund, D.C., Asimow, P.D., Farley, K.A., Rooney, T.O., Seeley, E., Jackson, E.W., Durhan Z.M., 2016. Enhanced East Pacific Rise hydrothermal activity during the last two glacial terminations. Science 351, 478. https://doi.org/10.1126/science.aad4296.
- Lund, D.C., Pavia, F.J., Seeley, E.I., McCart, S.E., Rafter, P.A., Farley, K.A., Asimow, P.D., Anderson, R.F., 2019. Hydrothermal scavenging of 230Th on the southern East Pacific rise during the last deglaciation. Earth Planet. Sci. Lett. 510, 64–72. https:// doi.org/10.1016/j.epsl.2018.12.037.
- Lyle, M., 1988. Climatically forced organic carbon burial in equatorial Atlantic and Pacific oceans. Nature 335, 529–532.
- Lyle, M., Marcantonio, F., Moore, W.S., Murray, R.W., Huh, C.-A., Finney, B.P., Murray, D.W., Mix, A.C., 2014. Sediment size fractionation and focusing in the equatorial Pacific: effect on 230Th normalization and paleoflux measurements. Paleoceanography 29, 2014PA002616. https://doi.org/10.1002/2014pa002616.
- Lyle, M., Mitchell, N., Pisias, N., Mix, A., Martinez, J.I., Paytan, A., 2005. Do geochemical estimates of sediment focusing pass the sediment test in the equatorial Pacific? Paleoceanography 20, PA1005. https://doi.org/10.1029/2004pa001019.
- Lyle, M., Pisias, N., Paytan, A., Martinez, J.I., Mix, A., 2007. Reply to comment by R. Francois et al. on "Do geochemical estimates of sediment focusing pass the sediment test in the equatorial Pacific?": further explorations of 230Th normalization. Paleoceanography 22, PA1217. https://doi.org/10.1029/2006PA001373.
- Mangini, A., Jung, M., Laukenmann, S., 2001. What do we learn from peaks of uranium and of manganese in deep sea sediments? Mar. Geol. 177, 63–78. https://doi.org/10. 1016/S0025-3227(01)00124-4.
- Marcantonio, F., Anderson, R.F., Higgins, S., Stute, M., Schlosser, P., Kubik, P., 2001. Sediment focusing in the central equatorial Pacific Ocean. Paleoceanography 16, 260–267. https://doi.org/10.1029/2000PA000540.
- Marchitto, T.M., Lehman, S., Ortiz, J., Fluckiger, J., vanGeen, A., 2007. Marine radiocarbon evidence for the Mechanism of deglacial atmospheric CO2 rise. Science 316, 1456–1459.
- Martínez, I., Keigwin, L., Barrows, T.T., Yokoyama, Y., Southon, J., 2003. La Niña-like conditions in the eastern equatorial Pacific and a stronger Choco jet in the northern Andes during the last glaciation. Paleoceanography 18, 1033. https://doi.org/10.

#### 1029/2002PA000877.

- Martínez-García, A., Sigman, D.M., Ren, H., Anderson, R.F., Straub, M., Hodell, D.A., Jaccard, S.L., Eglinton, T.I., Haug, G.H., 2014. Iron fertilization of the subantarctic ocean during the last ice age. Science 343, 1347–1350. https://doi.org/10.1126/science.1246848.
- McGee, D., Marcantonio, F., Lynch-Stieglitz, J., 2007. Deglacial changes in dust flux in the eastern equatorial Pacific. Earth Planet. Sci. Lett. 257, 215–230. https://doi.org/10. 1016/j.epsl.2007.02.033.
- McGee, D., Winckler, G., Borunda, A., Serno, S., Anderson, R.F., Recasens, C., Bory, A., Gaiero, D., Jaccard, S.L., Kaplan, M., McManus, J.F., Revel, M., Sun, Y., 2016. Tracking eolian dust with helium and thorium: impacts of grain size and provenance. Geochem. Cosmochim. Acta 175, 47–67. https://doi.org/10.1016/j.gca.2015.11.023.
- Mekik, F.A., Anderson, R.F., Loubere, P., François, R., Richaud, M., 2012. The mystery of the missing deglacial carbonate preservation maximum. Quat. Sci. Rev. 39, 60–72. https://doi.org/10.1016/j.quascirev.2012.01.024.
- Messié, M., Chavez, F., 2012. A global analysis of ENSO synchrony: the ocean biological response to physical forcing. J. Geophys. Res.: Oceans 117https://doi.org/10.1029/ 2012.IC007938
- Otto-Bliesner, B., Hewitt, C.D., Marchitto, T.M., Brady, E., Abe-Ouchi, A., Crucifix, M., Murakami, S., Weber, S.L., 2007. Last glacial maximum ocean thermohaline circulation: PIMP2 model intercomparisons and data constraints. Geophys. Res. Lett. 34. https://doi.org/10.1029/2007GL029475.
- Paytan, A., Kastner, M., Chavez, F.P., 1996. Glacial to interglacial fluctuations in productivity in the equatorial pacific as indicated by marine barite. Science 274, 1355–1357. https://doi.org/10.2307/2892054.
- Pedersen, T.F.K.-.Q., 1983. Increased productivity in the eastern equatorial Pacific during the last glacial maximum (19,000 to 14,000 yr B.P.). Geology 11, 16–19.
- Pedro, J.B., van Ommen, T.D., et al., 2011. The last deglaciation: timing the bipolar seesaw. Clim. Past 7, 671–683.
- Petit, J.-R., al, et al., 1999. Climate and atmospheric history of the past 420,000 years from the Vostok ice core, Antarctica. Nature 399, 429–436.
- Pichat, S., Sims, K.W.W., François, R., McManus, J.F., Brown Leger, S., Albarède, F., 2004. Lower export production during glacial periods in the equatorial Pacific derived from (231Pa/230Th)xs,0 measurements in deep-sea sediments. Paleoceanography 19, PA4023. https://doi.org/10.1029/2003PA000994.
- Pichevin, L.E., Reynolds, B.C., Ganeshram, R.S., Cacho, I., Pena, L., Keefe, K., Ellam, R.M., 2009. Enhanced carbon pump inferred from relaxation of nutrient limitation in the glacial ocean. Nature 459, 1114.
- Rafter, P.A., Sigman, D.M., Mackey, K.R.M., 2017. Recycled iron fuels new production in the eastern equatorial Pacific Ocean. Nat. Commun. 8, 1100. https://doi.org/10. 1038/s41467-017-01219-7.
- Rein, B., Lückge, A., Reinhardt, L., Sirocko, F., Wolf, A., Dullo, W.-C., 2005. El Niño variability off Peru during the last 20,000 years. Paleoceanography 20, PA4003. https://doi.org/10.1029/2004PA001099.
- Richaud, M., Loubere, P., Pichat, S., Francois, R., 2007. Changes in opal flux and the rain ratio during the last 50,000 years in the equatorial Pacific. Deep Sea Res. Part II Top. Stud. Oceanogr. 54, 762–771. https://doi.org/10.1016/j.dsr2.2007.01.012.
- Robinson, R.S., Sigman, D.M., DiFiore, P.J., Rohde, M.M., Mashiotta, T.A., Lea, D.W., 2005. Diatom-bound 15N/14N: new support for enhanced nutrient consumption in the ice age subantarctic. Paleoceanography 20, PA3003. https://doi.org/10.1029/2004PA001114.
- Rudnick, R.L., Gao, S., 2014. 4.1 composition of the continental crust. In: Turekian, H.D.H.K. (Ed.), Treatise on Geochemistry, second ed. Elsevier, Oxford, pp. 1–51. https://doi.org/10.1016/B978-0-08-095975-7.00301-6.
- Sarmiento, J.L., Gruber, N., Brzezinski, M.A., Dunne, J.P., 2004. High-latitude controls of thermocline nutrients and low latitude biological productivity. Nature 427, 56–60. https://doi.org/10.1038/nature02127.
- Sarnthein, M., Winn, K., Duplessy, J.-C., Fontugne, M.R.K.-Q., 1988. Global variations of surface ocean productivity in low- and mid-latitudes: influence on CO2 reservoir of the deep ocean and atmosphere during the last 21,000 years. Paleoceanogr 3, 361–399.
- Shimmield, G.B., Price, N.B., 1988. The scavenging of U,230Th and 231Pa during pulsed hydrothermal activity at 20°S, East Pacific Rise. Geochem. Cosmochim. Acta 52, 669–677. https://doi.org/10.1016/0016-7037(88)90329-8.
- Sigman, D., Boyle, E.A., 2000. Glacial/Interglacial variations in atmospheric carbon dioxide. Nature 407, 859–869.
- Sigman, D.M., Hain, M.P., Haug, G.H., 2010. The polar ocean and glacial cycles in atmospheric CO2 concentration. Nature 466, 47.
- Singh, A.K., Marcantonio, F., Lyle, M., 2011. Sediment focusing in the Panama basin, eastern equatorial Pacific Ocean. Earth Planet. Sci. Lett. 309, 33–44. https://doi.org/ 10.1016/j.epsl.2011.06.020.
- Stott, L., Poulsen, C., Lund, S., Thunell, R., 2002. Super ENSO and global climate oscillations at millennial time scales. Science 297, 222–226.
- Suman and Bacon, 1989. Variations in Holocene sedimentation in the North American Basin determined from <sup>230</sup>Th measurements. Deep-Sea Res. Part A Oceanogr. Res. Pap. 36 (6).
- Trathan, P., Forcada, J., Murphy, E., 2007. Environmental forcing and Southern Ocean marine predator populations. In: Antarctic Ecosystems. Philosophical Transactions of the Royal Society B, vol. 362. pp. 2351–2365.
- Tudhope, A., Chilcott, C.P., McCulloch, M.T., Cook, E.R., Chappell, J., Ellam, R.M., Lea, D.W., Lough, J.M., Shimmield, G.B., 2001. Variability in the El Niño-Southern oscillation through a glacial-interglacial cycle. Science 291, 1511–1517.
- van Oldenborgh, G.J., Burgers, G., 2005. Searching for decadal variations in ENSO precipitation teleconnections. Geophys. Res. Lett. 32, L15701. https://doi.org/10.1029/2005GL023110.
- Winckler, G., Anderson, R.F., Fleisher, M.Q., McGee, D., Mahowald, N., 2008. Covariant

- glacial-interglacial dust fluxes in the equatorial pacific and Antarctica. Science 320,
- 93–96. https://doi.org/10.1126/science.1150595.
  Winckler, G., Anderson, R.F., Jaccard, S.L., Marcantonio, F., 2016. Ocean dynamics, not dust, have controlled equatorial Pacific productivity over the past 500,000 years. Proc. Natl. Acad. Sci. Unit. States Am. 113, 6119-6124. https://doi.org/10.1073/ pnas.1600616113.
- Yang, H.-S., Nozaki, Y., Sakai, H., Masuda, A., 1986. The distribution of 230Th and 231Pa in the deep-sea surface sediments of the Pacific Ocean. Geochem. Cosmochim. Acta 50, 81-89. https://doi.org/10.1016/0016-7037(86)90050-5
- Yang, Y.-L., Elderfield, H., Pedersen, T.F., Ivanovich, M., 1995. Geochemical record of the
- Panama basin during the last glacial maximum carbon event shows that the glacial ocean was not suboxic. Geology 23, 1115-1118. https://doi.org/10.1130/0091-7613(1995)023<1115:grotpb>2.3.co;2.
- Yu, J., Anderson, R.F., Jin, Z., Rae, J.W.B., Opdyke, B.N., Eggins, S.M., 2013. Responses of the deep ocean carbonate system to carbon reorganization during the Last Glacial-interglacial cycle. Quat. Sci. Rev. 76, 39-52. https://doi.org/10.1016/j. quascirev.2013.06.020.
- Zheng, W., Braconnot, P., Guilyardi, E., Merkel, U., Yu, Y., 2008. ENSO at 6ka and 21ka from ocean-atmosphere coupled model simulations. Clim. Dyn. 30, 745-762. https:// doi.org/10.1007/s00382-007-0320-3.